ESOMAT 2009, 06016 (2009)
DOI:10.1051/esomat/200906016

Mechanical Behavior of a Metastable Austenitic Stainless Steel

P. Haušild[1,a], P. Pilvin[2] and M. Karlík[1]

[1]Czech Technical University in Prague, Faculty of Nuclear Sciences and Physical Engineering, Department of Materials, Trojanova 13, 120 00 Praha 2, Czech Republic
[2]Université de Bretagne-Sud, Laboratoire d'Ingénierie des Matériaux de Bretagne, Rue de Saint-Maudé, BP 92116, 56321 Lorient, France

Abstract. The mechanical properties of metastable austenitic steel corresponding to the AISI301 were characterized by means of tensile testing and cupping tests. High sensitivity to the strain rate was observed. The fracture mechanism in tensile specimens changed from the combination of cleavage and ductile dimpled rupture at lower strain rates to entire ductile dimpled rupture at higher strain rates. Fracture mechanisms were very different in deep drawn cups. After deep drawing tests, delayed cracking occurred. Main fractographic feature observed in cracked deep drawn cups was the intergranular decohesion.
The mechanical behavior was described by a two-phase model incorporating the martensitic transformation. Identification of parameters was carried out on complex loading paths (tensile test, shear test, cyclic loading-unloading).

1. Introduction

Austenitic stainless steels have an excellent corrosion resistance, good mechanical properties and are widely used for cold forming (deep-drawing) at room temperature. Increasing need for conserving the strategic elements such as nickel and chromium impel the steel-makers to lower the content of these elements in stainless steels. However, the low nickel content can lead during the forming process to the plastic deformation-induced phase transformation of face-centered cubic (fcc) γ austenite to body-centered cubic (bcc) α' martensite [1-4]. High internal stresses are generated due to an incompatible transformation strain accompanying the martensitic transformation. The residual stresses together with the internal stresses induced by martensitic transformation can lead after deep-drawing to the phenomenon of delayed cracking. Several authors mentioned the role of hydrogen in delayed cracking phenomena [5-7], e.g., increasing α' martensite content was found to have a huge effect on the hydrogen embrittlement susceptibility a cathodically charged AISI 304 austenitic stainless steel [5].

The aim of this paper is to characterize the influence of martensitic transformation on the mechanical properties of metastable austenitic steels and to propose numerical modeling of the material behavior in order to assess the local stress-strain field arising in each phase during plastic deformation.

2. Experimental results

The material chosen for this study was austenitic steel corresponding to the AISI301. The chemical composition is given in Table 1. The low nickel and chromium content situates the steel at the limit of the austenite field in the phase diagram. The material was provided as cold rolled sheets of 0.68 mm thickness in the bright annealed state.

Table 1. Chemical composition of AISI301 steel (in wt.%).

	C	Cr	Ni	Si	Mn	Mo
nominal	Max 0.12	16-18	6.5-9	<1.5	<2	<0.8
	0.05	17	7	0.5	1.5	0.1

[a] e-mail: petr.hausild@fjfi.cvut.cz

Article available at http://www.esomat.org or http://dx.doi.org/10.1051/esomat/200906016

The tensile tests were carried out on an INSPEKT 100kN testing machine at room temperature imposing various strain rates ranging from $\dot{\varepsilon}$ =5.10^{-5} s^{-1} to $\dot{\varepsilon}$ =5.10^{-2} s^{-1}. Temperature increase during tests was measured by a thermocouple. Cup drawing tests were carried out on a 500kN INSTRON testing machine using punch diameter 100 mm and different drawing ratios.

Fractured tensile specimens and cracked cups were examined in the Scanning Electron Microscope (SEM) JSM 5510LV. The martensite volume fraction was characterized by EBSD in SEM FEI Quanta 200 FEG equipped with a TSL™ EBSD analyzer. Acquired data were evaluated by OIM™ software.

2.1 Tensile tests

Results of tensile tests (in the rolling direction - RD) at room temperature with strain rates ranging from $\dot{\varepsilon}$=5.10^{-5} s^{-1} to $\dot{\varepsilon}$=5.10^{-2} s^{-1} are shown in Fig.1. The shape of stress-strain curves is strongly dependent on strain rate. With increasing strain rate yield stress increases, fracture stress and elongation to fracture have a maximum at $\dot{\varepsilon}$=5.10^{-3} s^{-1}. During the tensile tests at higher strain rates ($\dot{\varepsilon}$=5.10^{-3} s^{-1} and $\dot{\varepsilon}$=5.10^{-2} s^{-1}), the heating of specimens occurred (temperature increase up to 50°C).

Fracture surfaces of tensile specimens tested at the strain rates $\dot{\varepsilon}$=5.10^{-5} s^{-1} and $\dot{\varepsilon}$=5.10^{-4} s^{-1}, were oriented in perpendicular to the loading axis whereas the fracture surfaces of tensile specimens tested at the strain rates $\dot{\varepsilon}$=5.10^{-3} s^{-1} and $\dot{\varepsilon}$=5.10^{-2} s^{-1}, were inclined of about 45º.

Fractographic analysis of specimens broken at the strain rate $\dot{\varepsilon}$=5.10^{-5} s^{-1} and $\dot{\varepsilon}$=5.10^{-4} s^{-1} revealed several transgranular cleavage facets connected by ductile dimpled rupture (Fig. 2a). Several slip bands can be found on cleavage facets which indicate that the cleavage facets were formed before the final ductile fracture. On the other hand, the fracture surfaces of tensile specimens tested at the strain rates $\dot{\varepsilon}$=5.10^{-3} s^{-1} and $\dot{\varepsilon}$=5.10^{-2} s^{-1}, are completely covered by ductile dimples (Fig. 2b).

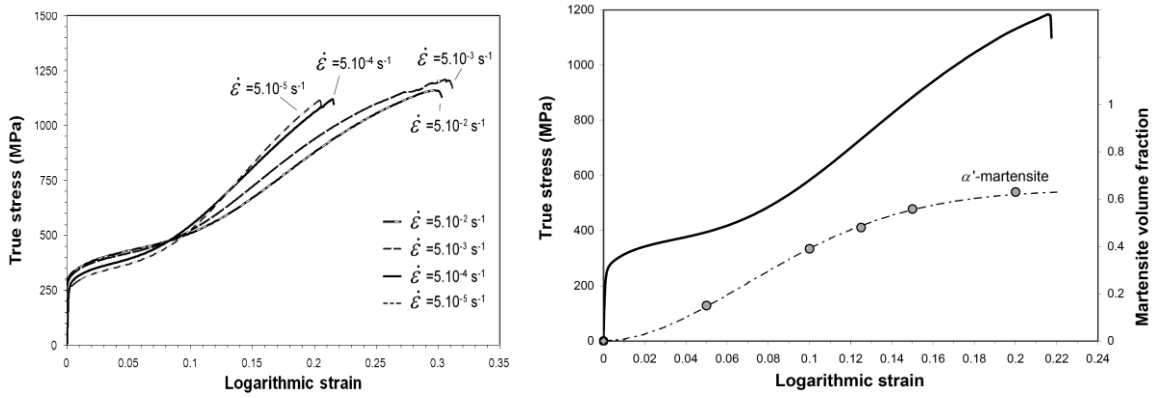

a) b)

Fig. 1. Stress-strain curves of AISI301 steel tested at room temperature at different strain rates (a), evolution of martensite volume fraction in the specimen tested at $\dot{\varepsilon}$=5.10^{-4} s^{-1}.

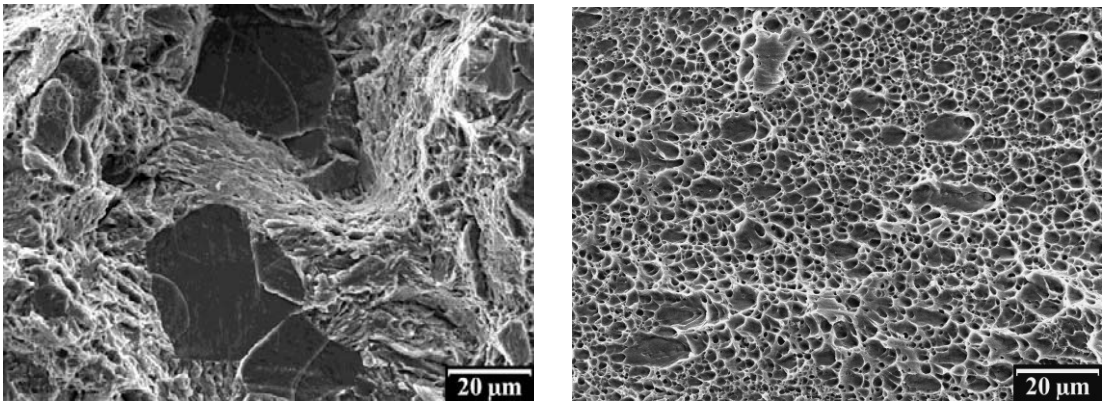

a) b)

Fig. 2. Fracture surfaces of tensile specimens tested at room temperature at $\dot{\varepsilon}$=5.10^{-4} s^{-1} (a), and $\dot{\varepsilon}$=5.10^{-3} s^{-1} (b).

2.1 Cupping tests

Delayed fracture occurred in the cups (Fig.3) after deep drawing tests with drawing ratios DR > 1.5. On the lateral face several more or less equidistant arrested cracks can be observed. Cracks arrested in the cup wall at about the same height as the height of cup with initial drawing ratio DR ~ 1.4.

Lateral faces and cracks in the cups issued from deep drawing tests were analyzed in SEM. Cracks propagated by the mechanism of diffused damage - several microcracks were found in proximity of principal crack lips and ahead of the crack tips (Fig.4a). On the fracture surfaces of opened cracks, the main feature observed was the intergranular decohesion (Fig.4b).

Fig. 3. Delayed cracking after deep drawing test in cups with different drawing ratios.

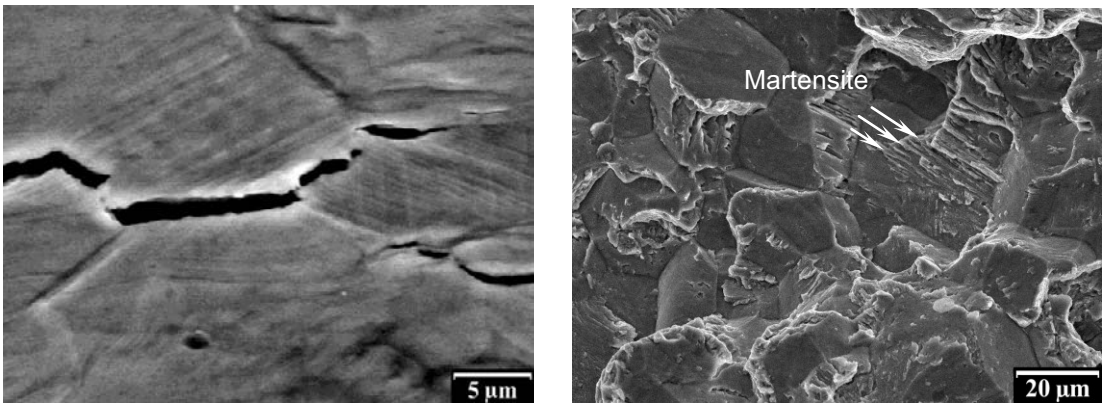

a) b)

Fig. 4. Crack propagation on the lateral face of the cup (a), intergranular decohesion on the fracture surface of the cup cracked after deep drawing test (b).

3. Numerical modeling

Constitutive equations for two-phase material have already been detailed in [8] and are only summarized here. The aim of this model is to characterize the behavior of the steel at a macroscopic scale by taking into account the individual behavior and the volume fraction of each phase (martensite: f_M and austenite: $1–f_M$). In this work, a self-consistent approach is used and it assumes that each phase is embedded in a homogeneous equivalent medium. The representative volume element is constituted here of two phases, i.e., austenite and martensite, and it is assumed that both phases have the same isotropic elastic behavior.

AISI 301 austenitic stainless steel undergoes a martensitic phase transformation induced by plastic deformation. The description of this transformation must be incorporated in the model in addition to the behavior of austenitic and martensitic phases.

3.1 Constitutive equations for austenite

In the initial state, the steel is 100% austenitic. Due to the orthotropic symmetry of the sheet, the austenite behavior is modeled as orthotropic, whereas the martensite behavior is described using isotropic behavior.

The yield stress function f for austenite is expressed in the form:

$$f\left(\sigma_a, X^a, R^a\right) = \sqrt{\left(\sigma_a^d - X^a\right) : \mathcal{H} : \left(\sigma_a^d - X^a\right)} - R_o^a - R^a \tag{1}$$

where ${\sigma_a}^d$ is the deviatoric part of the stress tensor in austenite. X^a is the second order tensor of kinematic work-hardening and R^a is the term of isotropic work-hardening. The initial yield stress ${R_o}^a$ is equal to the yield stress in tension along the RD and $\mathcal{H}$ is the fourth-order Hill's tensor. The coefficients of $\mathcal{H}$ can be deduced from the 6 parameters F, G, H, L, M and N of the quadratic Hill's criterion. The condition on the initial yield stress along the RD allows to impose the relation G + H = 1.
The viscoplastic strain follows a flow rule derived from a viscoplastic potential which is a power function of the yield function:

$$\frac{d\varepsilon_p^a}{dt} = \left(\frac{f^+}{K}\right)^n \frac{\partial f}{\partial \sigma} \tag{2}$$

where n is the strain rate sensitivity coefficient, K a weighting coefficient of the viscous part of the stress and f+ the positive part of f, i.e., f+=max(0, f). Hence, the behavior is elastic if $f < 0$.

The evolution of the isotropic work-hardening is associated to the dislocation density ρ in austenite:

$$R^a = M_T \alpha \mu b \sqrt{\rho} \qquad \text{with} \quad \frac{d\rho}{dt} = \frac{M_T}{b}\frac{dp^a}{dt}\left(\frac{1}{\Lambda} + k\sqrt{\rho} - bG\rho\right) \tag{3}$$

where M_T is the Taylor factor, α is a constant of the order of one, μ is the elastic shear modulus, b is the magnitude of Burger's vector and p^a is cumulative plastic strain in austenite. The first two terms in the bracket of eq.(3) represent the storage of dislocations in the microstructure, which may be interfered by obstacles as grain boundaries and/or by the average spacing between the forest dislocations. The third term in the bracket of eq.(3) takes into account the dynamical recovery process (annihilation of screw dislocations) assumed to be linear with ρ and characterized by a recovery coefficient G.

The kinematic hardening rule is similar to the well know Armstrong-Frederick law with the addition of a linear term:

$$X^a = \frac{2}{3}\left[C^a \alpha^a + H^a {\varepsilon^a}_p\right] \qquad \text{with} \quad \frac{d\alpha^a}{dt} = \frac{dp^a}{dt}\left(\frac{\partial f}{\partial \sigma} - \Gamma^a \alpha^a\right) \tag{4}$$

where parameters C^a and Γ^a control the intensity of work-hardening and H^a is the slope of the linear part of the kinematic work-hardening.

3.2 Constitutive equations for martensite

The martensite behavior is described using a simple elastoplastic model (von Mises criterion with a Voce law for isotropic work-hardening). The yield stress function g for martensite is expressed in the form:

$$g\left(\sigma_m, R^m\right) = \sqrt{\frac{3}{2}\sigma_m^d : \sigma_m^d} - R_o^m - Q^m\left[1 - \exp(-b^m p^m)\right]^{\frac{1}{2}} \tag{5}$$

where ${\sigma_m}^d$ is the deviatoric part of the stress tensor in martensite. ${R^m}_o$, Q^m, and b^m are hardening material parameters and p^m is cumulative plastic strain in martensite.

3.3 Austenite-martensite transformation

In this work, the evolution of the volume fraction of martensite is given by the Shin et al. law [10], in which the martensitic transformation is considered as a continual relaxation of the internal strain energy accumulated during the plastic deformation. This volume fraction depends on the cumulative plastic strain in the austenite (p^a) and not on the macroscopic strain. Furthermore, it is clearly established that the kinetic of the martensitic transformation depends on the temperature and stress path [9].
In order to take into account the transformation dependence on the stress path, the evolution of the austenite-martensite transformation depends on the stress triaxiality ratio in austenite (T^a). This ratio is equal to 0 in shear,

1/3 in tension. The evolution law of the martensite volume fraction f_M is expressed in eq.(6) where f_M^∞ is the value of the saturation of the martensite volume fraction. In the evolution rate of the transformation, the dependence of the stress triaxiality ratio is introduced with linear functions: $f_M^\infty(T^a)$ and $\beta(T^a)$.

$$\frac{df_M}{dt} = \frac{dp^a}{dt}\left[f_M^\infty(T^a) - f_M\right]\beta(T^a)N\, p^{a\,(N-1)} \tag{6}$$

In equation (6) the value of the exponent N is about 2 according to [10].

3.4 Parameters identification

Parameters were identified using identification software SiDoLo based on a Levenberg–Marquardt minimization algorithm [11]. The experimental database consists of monotonic shear tests and tensile tests (along rolling and transverse directions) at room temperature with different strain rates (Fig.5a). Cyclic shear tests are used to identify the kinematic hardening parameters (Fig.5b). Identified model of material behavior is in good agreement with monotonic tensile and/or shear test and cyclic shear test results (Fig.5) as well as with austenite to martensite transformation kinetics during tensile and shear tests (Fig.6).

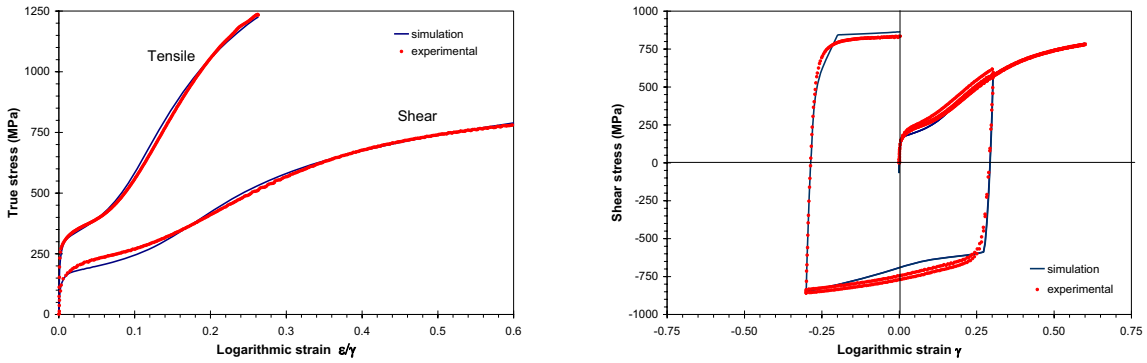

a) b)

Fig. 5. Identification of material behavior on monotonic tensile and shear tests (a) and cyclic shear tests (b).

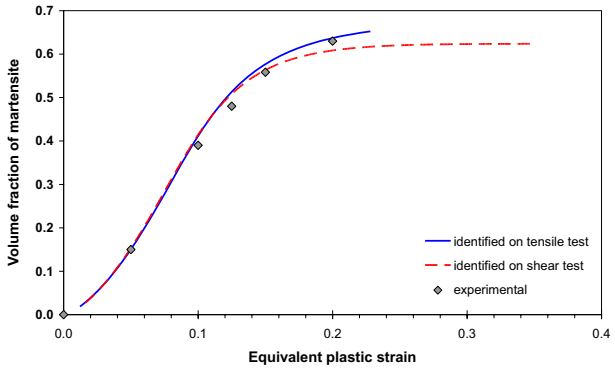

Fig. 6. Identification of austenite to martensite transformation kinetics on monotonic tensile and shear tests.

4. Summary

Mechanical response of AISI301 steel is very sensitive to the strain rate due to the coupling of thermo-mechanical behaviors. Fracture mechanism in tensile specimens at the strain rate lower than $\dot{\varepsilon}=5.10^{-3}$ s^{-1} is the combination of cleavage and ductile dimpled rupture. At the strain rate higher than $\dot{\varepsilon}=5.10^{-3}$ s^{-1} fracture mechanism changes to entire ductile dimpled rupture.

Fracture mechanisms are very different in tensile specimens and deep drawn cups. In cracked deep drawn cups, the intergranular decohesion was main fractographic feature.
Delayed cracking occurred only in deep drawn cups but not in tensile specimens. This is probably due to the necessity of the synergy effect between macroscopic (residual) stresses and internal stresses provoked by martensitic transformation.
The mechanical behavior was described by a two-phase model incorporating the individual behavior and the volume fraction of each phase. Identification of model parameters was successfully carried out on complex loading paths (monotonic tensile and shear test, cyclic shear test).
In the following research, the model will be implemented in a finite element method code and used for the simulation of cupping test.

Acknowledgement

Authors wish to thank the Arcelor-Mittal group for supplying the material. This work was supported by the Ministry of Education, Youth and Sports of the Czech Republic in the frame of the research project MSM 6840770021. Authors are deeply grateful to Dr S. Bouvier (LPMTM, Villetaneuse) who kindly provided experimental data for cyclic shear tests.

References

[1] L. Mangonon Jr., G. Thomas, Met. Trans. 1 (1970) 1577–1586.
[2] T. Suzuki, H. Kojima, K. Suzuki, T. Hashimoto, M. Ichihara, Acta Met. 25 (1977) 1151–1162.
[3] J.W. Brooks, M.H. Loretto, R.E. Smallman, Acta Met. 27 (1979) 1839–1847.
[4] M. Humbert, B. Petit, B. Bolle, N. Gey, Mater. Sci. Eng. A 454–455 (2007) 508–517.
[5] H. Hanninen, T. Hakarainer, Corrosion 36 (1980), 47-51.
[6] J.A. Brooks, A.J. West, Metall. Trans. A 12 (1981), 213-223.
[7] C. Pan, W.Y. Chu, Z.B. Li, D.T. Liang, et al., Mater. Sci. Eng. A351 (2003) 293-298.
[8] S. Gallée, P.Y. Manach, P. Pilvin, S. Thuillier, G. Lovato, Matériaux et Techniques, 3-4, (2003) 1-10
[9] A.A. Lebedev, V.V. Kosarchuk, International Journal of Plasticity, 16, (2000) 749-767.
[10] H.C. Shin, T.K. Ha, Y.W. Chang, Scripta Materialia, 45, (2001) 823-829.
[11] Ph. Pilvin, in: Proc. of MécaMat, C. Oytana *et al* editors (1988) 155-164.